Analytical Discussion on Dynamics of Inverter-Based Resources under Small-Signal Conditions

Johanna Vorwerk*§, Mehdi Ghazavi Dozein‡, Pierluigi Mancarella‡, and Gabriela Hug*
*Power Systems Laboratory, ETH Zürich, Zürich, Switzerland
‡ School of Electrical and Electronic Engineering, The University of Melbourne, Melbourne, Australia
§vorwerkj@ethz.ch

***Abstract*—Grid integration of inverter-based resources (IBRs) and the consequent phase-out of synchronous machines cause a reduction in system strength and inertia, which may pose system instability challenges, including small-signal and inverter-driven instability. There is an ongoing discussion on the contributing factors to IBR stability, synchronism, and response specifications (e.g., response time, damping) under various grid conditions and characteristics. This paper presents an analytical discussion highlighting how grid characteristics such as short-circuit ratio, R/X ratio, and system loading conditions may affect IBR stability and synchronism under small-signal conditions. Furthermore, the contributing factors to IBR response characteristics imposed by the external grid are identified. The analytical discussion highlights the need to consider such factors when determining grid-code requirements for IBR response specifications and stability conditions.**

***Index Terms*—- Power system dynamics, IBR, Small-signal analysis, Weak grid, IBR stability.**

I. Introduction

Power systems worldwide undergo a substantial transition as the penetration of inverter-based resources (IBRs), including generation and loads, is expected to rise tremendously in the coming years. The reduction of inertia associated with replacing synchronous machines increases the need for frequency stability support and fast frequency response provision. In addition, the phase-out of synchronous machines reduces the short-circuit current, which weakens the system and can result in system strength challenges, including IBR instability and disconnection [1, 2]. Hence, it is essential to understand how to ensure IBR stability and synchronism under various grid characteristics and operating conditions.

There is an ongoing discussion aiming to define response specifications for IBRs, also called IBR grid-code requirements, to guarantee their inverter-driven stability while enhancing overall power system stability during abnormal conditions such as system contingencies and faults [3, 4]. In the literature, IBR stability and its response specifications are mainly discussed on a device level, while potential issues emerging from the external system are yet to be understood. For example, [5, 6] identify how converter control schemes enhance IBR stability but neglect system-level impacts. On the other hand, grid codes define IBR response functionalities such as power factor control, ride-through response, momentary cessation, or angle jump requirements while ignoring how the IBR performance may be influenced by external grid operating conditions [7–9].

Literature suggests that IBR control schemes and their stable operation may be affected by the grid characteristics at the connection point, which substantially vary with the voltage level. In particular, the short-circuit ratio (SCR) significantly affects the stable space for droop and virtual inertia emulation control parameters, as highlighted through eigenvalue analysis in [10]. Furthermore, [11] presents fundamental transfer functions to analyze the limitations of dynamic support from IBRs in weak systems. Although the authors acknowledged the dependency on grid impedance and pre-disturbance operating conditions, they do not explore the effect of external grid characteristics and operating points on IBR stability.

Recent events in the Australian power system highlight that IBR stability and response compliance are severe concerns in the real-life renewable-rich system. In 2020, voltage oscillations caused challenges in maintaining stable IBR operation in the West Murray TN [12]. Significant oscillations were observed at the active/reactive power outputs of IBRs, which led to significant renewable curtailment enforced by the Australian system operator to ensure system-level stability. In addition, the events reported in [13] suggest that the external system operating conditions may influence and threaten stable IBR operation and response. Even so, an analytical and systematic discussion of such dynamic challenges and their root cause is lacking.

Extending the IBR mathematical framework derived in [11], this work explores how diverse grid conditions typical for different voltage levels might lead to undesirable or unstable operating conditions of IBRs. As such, the contributions of the presented work are threefold:

- First, we present an analytical discussion highlighting the contributing factors to IBR stability and synchronism under small-signal conditions, particularly those imposed by the external power system characteristics, including R/X ratio, grid strength, and voltage angle.
- Furthermore, we perform a small-signal analysis of the derived transfer functions to investigate how the system-level characteristics and operating conditions, such as R/X ratio, grid strength, and voltage angle, impact IBR response characteristics.
- Finally, we present implications of the results for real-world systems that highlight the need to further analyze the dependencies to ensure IBR stability and desirable dynamic response under small-signal conditions.

II. General Small-Signal Model for IBRs

This section derives transfer functions that describe the current dynamics of an arbitrary grid-connected IBR. Then, the validity of the derived transfer functions and required assumptions are discussed. Finally, potential operating regimes for the given system are assessed to define parameterizations for the subsequent small-signal analysis.

The following notation is adopted for the presented work: Phasor approximation is assumed to hold for the provided system and dq-decomposition of currents and voltages applies and is indicated through corresponding subscripts. All system quantities and variables are formulated in per unit, represented by small letters (e.g. v, r, ℓ), except for the voltage angle.

A. Derivation of Transfer Functions

Various IBRs provide system services at different voltage levels in modern power systems. In general, both inverter-interfaced load and generation may adapt their active and/or reactive power setpoints following system disturbances. Fig. 1 shows a simplified but general grid connection of an IBR and defines the convention applied in this work: An IBR is connected to the power grid in parallel to a load. The load accounts for local consumption while $i_l = 0$ corresponds to a no-local-loading condition.

The transmission network (TN) is considered with an equivalent impedance (r_{TN},ℓ_{TN}) in series with a voltage source. The entire corridor, including lines and transformers in between the IBR terminal and the interface to the TN, is represented by the equivalent impedance (r_{DN}, ℓ_{DN}). The TN internal voltage source is modeled with its magnitude e_d and provides the reference angle. The voltage at the IBR terminal is described by its magnitude V and phase angle θ.

Applying the sign convention in Fig. 1 and phasor approximation, i.e. $i(t) = i_{dq}e^{j\omega_s t}$, the dynamic equations for the current are formulated as:

$$\begin{aligned} \frac{\ell}{\omega_b}\frac{di_d}{dt} &= e_d - v\cos(-\theta) - ri_d + \omega_s \ell i_q, \\ \frac{\ell}{\omega_b}\frac{di_q}{dt} &= -v\sin(-\theta) - ri_q - \omega_s \ell i_d, \end{aligned} \tag{1}$$

where $r = r_{\mathrm{DN}} + r_{\mathrm{TN}}$ and $\ell = \ell_{\mathrm{DN}} + \ell_{\mathrm{TN}}$ are the resistance and inductance seen from the IBR point of common coupling (PCC) in per unit, the base frequency is $\omega_b = 2\pi f$, and the synchronous frequency ω_s is expressed in per unit.

Small-signal disturbances cause deviations in the voltage magnitude and angle at the PCC that are followed by an initially uncontrolled and, depending on the control time constants, delayed control reaction of the IBR. While traditionally voltage and angle were decoupled and studied individually, weak systems exhibit disruptions in both quantities simultaneously [11]. Mathematically, such a small-signal disturbance is described by the pre-contingency quantity identified through subscript 0 and the deviation from the pre-fault condition indicated through Δ-notation. Replacing the per-unit inductance with its per-unit reactance $x = \ell$, using the grid impedance $z = \sqrt{x^2 + r^2}$ and expressing the resistance through the R/X ratio $k = r/x$, the small-signal model is expressed in terms of the grid impedance and R/X ratio at the IBR's PCC:

$$\begin{aligned} &\Delta i_d = G_1\Delta\theta + G_2\Delta v, \quad \Delta i_q = G_3\Delta\theta + G_4\Delta v, \\ &G_1 = \frac{v_0\omega_b\sqrt{1+k^2}}{z}\frac{(s+k\omega_b)\sin\theta_0 + \omega_s\omega_b\cos\theta_0}{(s+k\omega_b)^2 + (\omega_s\omega_b)^2}, \\ &G_2 = -\frac{\omega_b\sqrt{1+k^2}}{z}\frac{(s+k\omega_b)\cos\theta_0 - \omega_s\omega_b\sin\theta_0}{(s+k\omega_b)^2 + (\omega_s\omega_b)^2}, \\ &G_3 = \frac{v_0\omega_b\sqrt{1+k^2}}{z}\frac{(s+k\omega_b)\cos\theta_0 - \omega_s\omega_b\sin\theta_0}{(s+k\omega_b)^2 + (\omega_s\omega_b)^2}, \\ &G_4 = \frac{\omega_b\sqrt{1+k^2}}{z}\frac{(s+k\omega_b)\sin\theta_0 + \omega_s\omega_b\cos\theta_0}{(s+k\omega_b)^2 + (\omega_s\omega_b)^2}. \end{aligned} \tag{2}$$

The transfer functions are similar. Namely, it holds $G_3 = -v_0 G_2$ and $G_1 = v_0 G_4$. This proportionality suggests that amplitudes differ for each pair while the dynamic properties are equivalent. In other words, the d-axis current response to a change in angle is equivalent to a change of the q-axis current following a disruption in the voltage magnitude. As such, the dynamic coupling between the following quantities is similar: (i) Δi_d-$\Delta\theta$ and Δi_q-ΔV, (ii) Δi_d-ΔV and Δi_q-$\Delta\theta$.

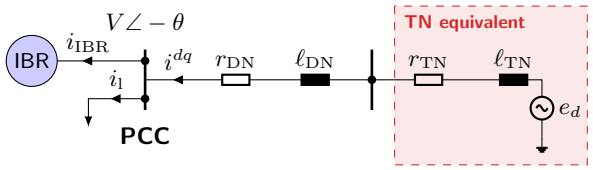

Fig. 1. General connection of an IBR to the grid. Note the selected convention of currents and voltage arrows.

B. Validity and Assumptions

Phasor approximation is required for the formulation provided in (1), assuming that currents and voltages are narrow-band signals around the nominal frequency. This assumption might be invalid for power systems with high penetration of IBRs in weak grid conditions. Especially during system transients, physical states in inverter-dominated power systems are more likely to be broad-band signals, as shown for real events in Australia [14, 15].

The formulation in (1) captures the reaction of the IBR currents to a change of the voltage magnitude and angle without making any assumptions on the inverter control. Thus, they apply for any IBR before the control affects the currents. Ancillary services are subsequent as they exhibit slower reactions. As such, the derived transfer functions capture the effect of grid characteristics on the initial response of any IBR, independent of the implemented control scheme.

Besides employing (2) to assess the dynamic response of IBRs, we can study them in reversed direction and assess how small changes in the IBR current affect the local grid. In this case, the control option of the IBR matters. If the IBR performs grid-feeding control, it synchronizes with the PCC's voltage angle, and the loading condition determines the angle. However, if a grid-forming concept is adopted, the IBR and the loading condition affect the PCC angle. This grid-forming case is not captured in the transfer functions. Thus when assessing (2) in reversed fashion, the results are valid for grid-feeding control only.

C. Operating Regimes

Due to different load and generation patterns, distinct operating conditions for IBR operation exist. If the IBR in Fig. 1 consumes power ($i_{\mathrm{IBR}} > 0$), e.g., as a load or a battery, the current i_{dq} is strictly positive. Power flows from the upstream network towards the IBR terminal, the voltage phasor at the IBR terminal lags compared to the Thevenin equivalent, and the angle θ is positive. Supposing the IBR is a generator, e.g., a PV system or a generating battery, two possibilities exist: If the local load exceeds generation at the IBR terminal, i.e., $|i_{\mathrm{IBR}}| < |i_l|$, power still flows from the upstream network into the IBR terminal. Thus current i^{dq} and angle θ are still positive. However, if the load is smaller than the IBR generation, i.e., $|i_{\mathrm{IBR}}| > |i_l|$, the power flow is inverted, resulting in an adverse current and a negative angle. As a result, positive and negative currents i_{dq} and angles θ are realistic and depend on the operating condition.

While grid codes define acceptable ranges for voltage magnitudes and typically require $V_0 \in [0.9, 1.1]$p.u., the initial angle depends on the loading condition of the grid. To ensure angular stability, voltage angles are required to stay within a secure angle region, within $\pm 90° \mp \varepsilon$, where ε represents an additional stability margin [16]. While small angle values,

around $0°$ reference value, indicate low loading conditions, larger angle values indicate high loading patterns.

As suggested by (2), the dynamics of the current being exchanged between IBR and the external grid follow second-order transfer functions right after the contingency and solely depend on some distinct grid characteristics. Besides the pre-fault voltage angle and magnitude, these include the R/X ratio and the grid impedance at the PCC. The latter two generally differ between voltage levels but can also substantially vary within one voltage level. TNs exhibit low R/X ratios, and system losses are usually insignificant. On the other hand, distribution networks (DNs) typically exhibit non-negligible losses that manifest in higher R/X ratios, above 0.5 or closer to 1 [16, 17].

The grid impedance correlates with the short-circuit power at the PCC and traditionally changes with the size of the system and grid strength [17]. Weak systems exhibit low fault levels, which manifests itself in low short-circuit ratios (SCR), e.g., SCR values less than $3\,\mathrm{p.u.}$, and high grid equivalent impedance, while the opposite holds for strong grids [8].

III. Dynamic Properties of IBR Responses under Small-Signal Conditions

This section contains a detailed small-signal analysis of the second-order IBR response developed in (2) considering the operating regimes discussed in Section II-C. First, it compares the derived model against a standardized 2nd order system formulation that permits general conclusions regarding the speed and damping of IBR responses under diverse grid conditions. Then, it provides exemplary bode plots and step responses for distinct grid characteristics.

A. Comparison to 2nd Order Standard Form

General conclusions arise when comparing systems to a standardized 2nd order formulation commonly studied in control theory. Analytically formulating its coefficients permits quantifying the system damping, response time, and overshoot depending on grid quantities.

1) Standard 2nd Order System with one Zero: Any 2nd order system with a zero can be expressed in terms of the following standard form [18]:

$$H(s) = K\frac{s/(\alpha\zeta\omega_n)+1}{(s/\omega_n)^2+(2\zeta/\omega_n)s+1}, \tag{3}$$

where K is the steady-state gain, ζ the damping factor, ω_n the natural frequency, and α positions the zero.

These coefficients provide an estimate for time-domain specification like the rise time t_r, settling time t_s, overshoot M_p and peak time t_p of a system. A general introduction to such systems and the effect of the coefficients on the dynamic performance is provided in [18].

2) Analysis of the Coefficients: By rearranging (2), the coefficients of the standard 2nd order system and the time-domain specifications can be extracted. Table I displays the analytic results. While resonance frequency, damping factor, and time-domain characteristics solely depend on the R/X ratio, the position of the zero, hence α, additionally depends on the voltage angle. Note that the peak time is a constant.

Fig. 2 depicts the time-domain characteristics for different grid characteristic parameters, while Fig. 3 displays the coefficients. The expected rise times are below $6\,\mathrm{ms}$, and the settling times do not exceed $100\,\mathrm{ms}$ for most R/X ratios, ensuring that the analysis is suitable for any controlled or uncontrolled IBR in grids with R/X¡0.15 as discussed in Section II-B.

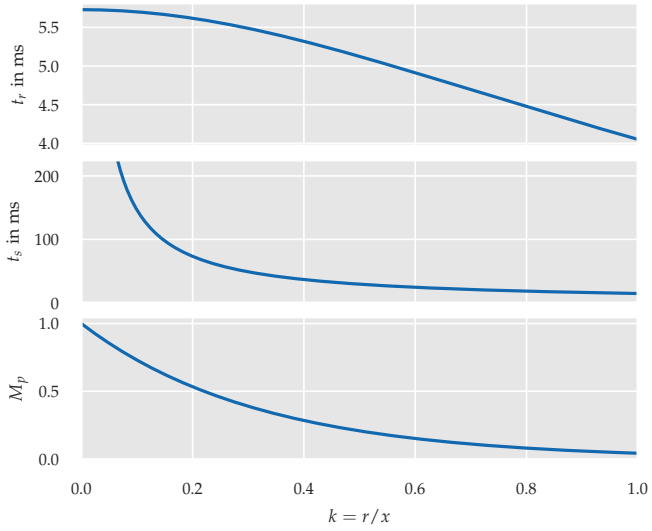

Fig. 2. Time domain characteristics of the transfer functions. Note that these are only valid when $|\alpha| \leq 3$ and may substantially vary otherwise.

Some meaningful differences are observed for different R/X ratios. The natural frequency and damping factor rise as k increases, causing lower overshoots, and shorter rise, and settling times. Consequently, oscillatory time responses with high overshoots of up to two times the new steady-state (i.e. $M_p = 1$) are expected for TNs with small R/X. Note that increased damping for higher R/X, hence DNs, correlates with diminishing overshoots and shorter settling times. As such, IBRs placed in DNs exhibit higher damping, and the time domain response settles quicker than for IBRs in TNs.

The location of the zero, hence the value of α, may affect the dynamic properties. While its placement does not affect the system's stability, an RHP zero causes non-minimum-phase behavior, an initially inverted response. As such, the zero significantly affects the dynamic properties of the system if it is close to the poles, i.e., $\alpha \approx 1$. In that case, the rise time of the system is significantly reduced, indicating a faster responding system. In addition, the overshoot is enhanced. On the other hand, a large α indicates that the zero is far from the poles of the system, and the effect of the zero diminishes. When the zero moves to the origin of the complex plane, it causes a direct, almost derivative behavior between the input and the output with immediate responses [18].

Fig. 3 suggests under which conditions the zero affects the time-domain characteristics. In all cases, operating conditions exist that cause non-minimum-phase behavior, as suggested

TABLE I
Coefficients and Time-Domain Performance Characteristics.

Parameter	Valid for	Expression
Resonance ω_n	G_1 to G_4	$\omega_b\sqrt{(k^2+\omega_s^2)}$
Damping ζ	G_1 to G_4	$k/\sqrt{(k^2+\omega_s^2)}$
α	G_1, G_4	$1+\omega_s/(k\tan\theta_0)$
	G_2, G_3	$1-\omega_s/k\tan\theta_0$
Rise time t_r	G_1 to G_4	$1.8/(\omega_b\sqrt{k^2+\omega_s^2})$
Peak time t_p		π/ω_b
Settling time t_s		$4.6/(k\omega_b)$
Overshoot M_p		$\exp(-\pi k)$

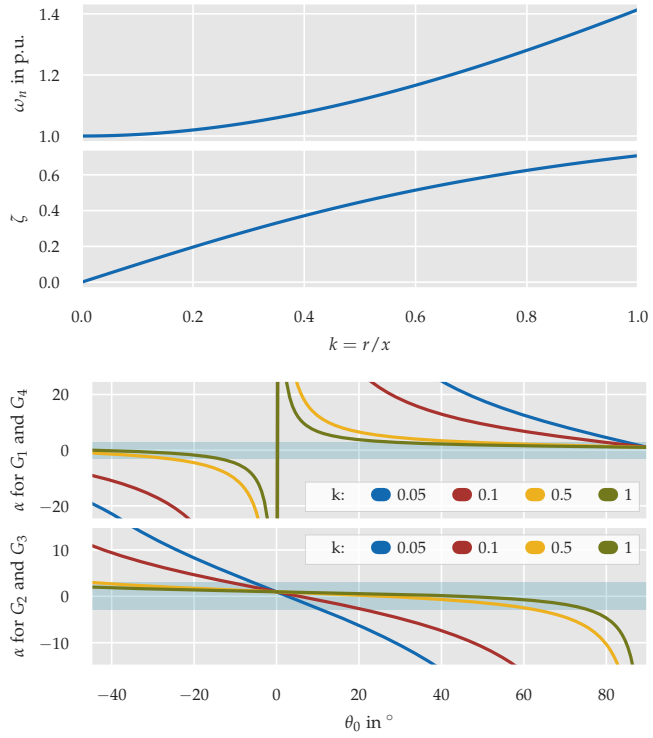

Fig. 3. Coefficients of the 2nd order standard transfer function for different R/X ratios and initial angles. All are independent of the initial voltage and grid impedance as indicated by Tab. I. The shaded areas mark $\alpha \in [-3, 3]$.

by $\alpha < 0$. For G_1 and G_4, the zero is only expected to affect the time-domain characteristics for high-loading scenarios, i.e., significant positive and negative initial angles and high R/X ratios. For small initial angles, a singularity occurs, i.e., α approaches infinity for 0°, indicating that the conclusions for low loading conditions and the time-domain response characteristics are extremely sensitive to the parameters of the system.

For G_2 and G_3, α heavily depends on the R/X ratio. For small R/X, the zero is only close to the origin for low loading conditions and quickly moves away from the origin as the angle increases or decreases. Thus, for TNs, an instant reaction between i_d and V, or i_q and θ, is only expected for low loading conditions, and the analytic description of the time-domain characteristics is valid. For IBRs in DNs, the situation differs. α stays close to unity for almost all loading conditions. Thus, the overshoot under these conditions is expected to increase compared to the values provided in Fig. 2.

B. Bode Plot Analysis

Fig. 4 provides the bode diagrams for all transfer functions and different R/X values. G_1 and G_4 are identical, thus shown in the same plot. Despite the same gain for G_2 and G_3, their phases are shifted by 180° due to the inversion in (2).

All amplitude responses exhibit a resonance close to the nominal frequency. On the one hand, this ensures controllability. If the system operated above its resonance, the gain would be reduced, preventing currents from following a voltage angle or magnitude change. Large control gains would be required to ensure suitable reactions in such a scenario. On the other hand, the resonance is enhanced for low R/X ratios, making overshoots and oscillatory behaviors more likely for TNs. At the same time, due to the high inherent gains in TNs, smaller

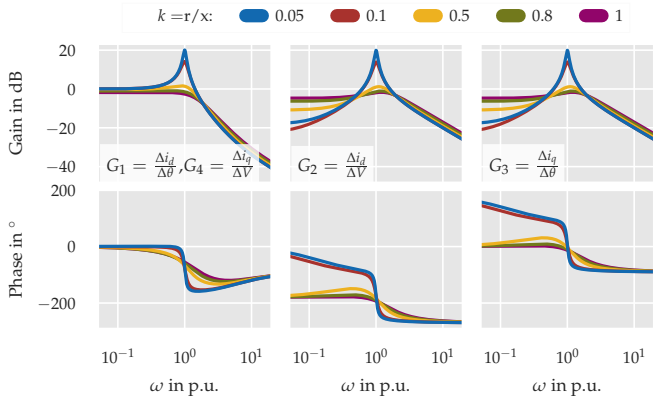

Fig. 4. Bode plots of the transfer functions for different R/X ratios for $v_0 = 1$ p.u. G_1 and G_2 on the left, G_3 in the middle and G_4 on the right.

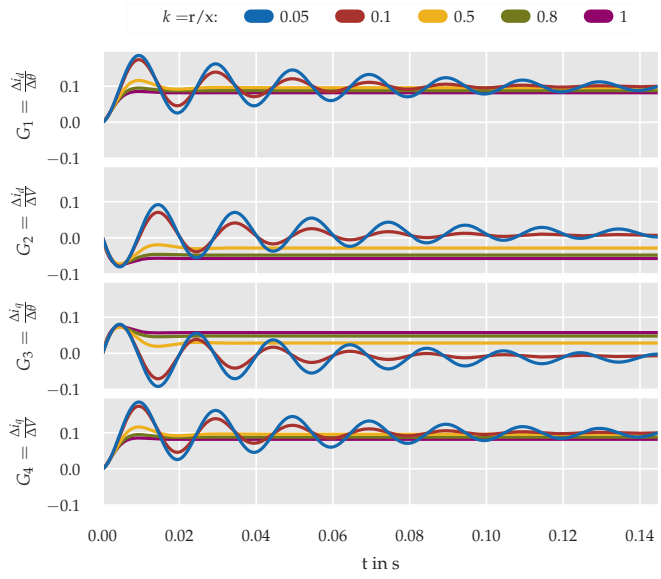

Fig. 5. Step response of the transfer functions G_1 to G_4 for a 0.1 p.u. input step for different R/X ratios and the constant parameters $v_0 = 1$ p.u., $\theta_0 = 10°$ and $z = 1$ p.u.

control reactions are required to control the output variable, while higher gains might be required for DNs.

C. Exemplary Step Response

Fig. 5 displays dynamic responses to a 0.1 p.u. step in the input and varying R/X ratios while keeping all other parameters constant at $v_0 = 1$ p.u., $\theta_0 = 10°$ and $z = 1$ p.u.. Some of the previous findings are evident: G_1 and G_4 exhibit the same response, because $v_0 = 1$ p.u.. Furthermore, G_2 is the inversion of G_3, and the peak times are approximately equal as suggested by Tab. I.

Fig. 5 clearly illustrates the dependence of the damping on the R/X ratio. TNs with low R/X ratio are prone to oscillations and higher overshoots of up to twice the post-fault steady-state magnitude. Similar findings hold for the settling time. The smaller the R/X ratio, the longer oscillations exist. On the contrary, DNs, with their higher k, exhibit smaller overshoots, and shorter settling times and thus provide more damping.

In addition, Fig. 5 confirms the standard $P\theta$, and QV-decoupling applied in traditional TN control concepts. Considering a typical R/X ratio of $k = 0.1$, the steady-state deviation

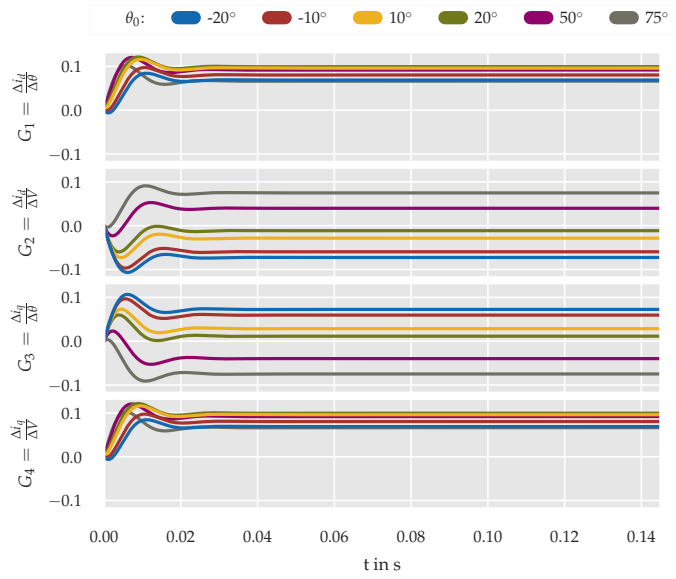

Fig. 6. Step response of the transfer functions G_1 to G_4 for a 0.1 p.u. input step for different initial angles θ and constant parameters $v_0 = 1$ p.u., $k = 0.5$ and $z = 1$ p.u.

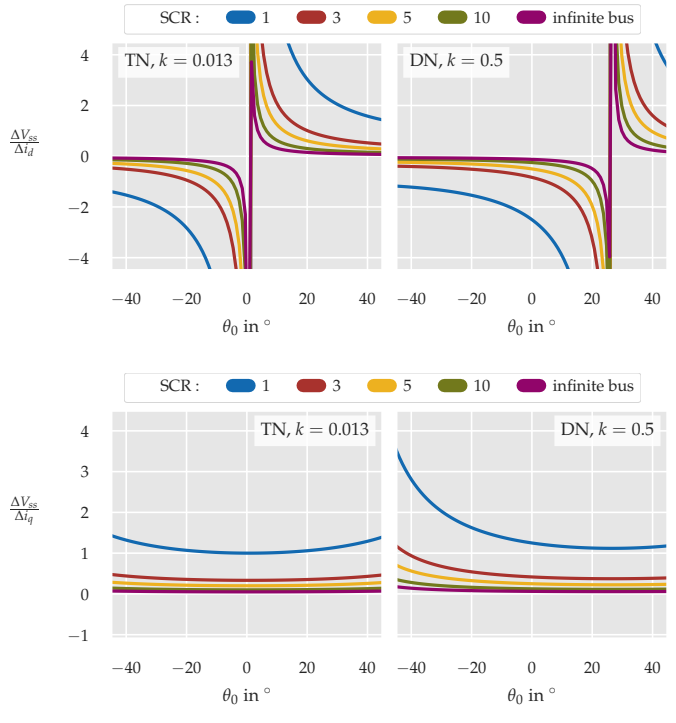

Fig. 7. Steady-state voltage deviation depending on the initial angle for different short circuit ratios (SCR= $1/x$). Dependency for Δi_d on the top and Δi_q on the bottom.

following a change in voltage magnitude is almost zero for the d-axis current, while it is maximal for the q-axis current. This indicates adequate controllability of voltage magnitudes through q-axis current, which is typically aligned with reactive power control. Similar findings hold for a change in the angle, ergo frequency, the d-axis current, and active power control. The decoupling is no longer valid for R/X ratios in the DN range, i.e. closer to unity. A disruption in voltage magnitude is followed by a significant steady-state deviation in both currents. The same holds for an angle disruption.

Fig. 6 shows step responses for different pre-fault loading conditions expressed in terms of varying θ_0, for $k = 0.5$. As predicted from the previous analysis, θ mainly affects the zero placement and thus does not significantly affect the damping and time constants - however, the steady-state reaction changes. A general trend appears for G_2 and G_3: the more the angle deviates from zero, i.e., the higher loaded the system, the larger the steady-state deviation. In other words, the higher the exchange between IBR and the external system, the more inaccurate the assumption of decoupling between P and V as well as Q and θ.

IV. Effects of IBR Control

System operators typically require IBRs to contribute to system frequency and voltage control. Hence, they adjust their power consumption or production following a change in local voltage magnitude or frequency. Especially in weaker systems, the voltage deviations caused by IBRs that provide frequency response are of concern [11]. Considering a grid-following IBR, the derived transfer functions are reformulated to compute the steady-state voltage magnitude change following an adjustment in current. Extending the formulation in [11], this section first formally derives the expected steady-state voltage magnitude deviation caused by IBR current control before analyzing it systematically under different grid operating conditions.

A. Derivation

The voltage change following an IBR current adjustment is obtained by inverting G_2 and G_4. Computing $s \to \infty$ provides the expected deviation in steady-state voltage magnitude Δv_{ss} for a change in the two currents:

$$\begin{aligned} \Delta v_{ss} &= \lim_{s\to 0} \frac{1}{G_2} \Delta i_d = -\frac{1}{\eta} \frac{k^2 + \omega_s^2}{k \cos\theta_0 - \omega_s \sin\theta_0} \Delta i_d, \\ \Delta v_{ss} &= \lim_{s\to 0} \frac{1}{G_4} \Delta i_q = \frac{1}{\eta} \frac{k^2 + \omega_s^2}{k \sin\theta_0 + \omega_s \cos\theta_0} \Delta i_q, \end{aligned} \tag{4}$$

where $\eta = x^{-1}$ is the short-circuit ratio (SCR) of the grid.

B. Critical Initial Operating Conditions

For both currents, a condition exists so that the denominator in (4) vanishes. Consequently, the change in voltage at this point is theoretically infinite. In real systems, it indicates that the local voltage is extremely sensitive to changes in current. Since the point only depends on the initial angle and R/X, we define the critical angle θ_0^{crit} as the angle at which the gain becomes infinite for a specific k:

$$\theta_{0,i_d}^{\text{crit}} = \arctan\left(k/\omega_s\right), \quad \theta_{0,i_q}^{\text{crit}} = \arctan\left(-\omega_s/k\right). \tag{5}$$

C. Effect of Grid Characteristics

Generally, (4) indicates that the voltage deviation solely depends on the SCR, R/X ratio, and the initial loading condition. Fig. 7 displays the expected change in voltage magnitude depending on grid characteristics.

In all cases, weaker grids with low SCR exhibit higher voltage deviations following a current control action. At the same time, this conclusion suggests that smaller control gains are required for local voltage control. However, when minor current adaptions significantly impact local voltages, they limit the amount of current that can be provided for ancillary services while still keeping the voltage magnitude within bounds. In some conditions, the gain exceeds 1, indicating

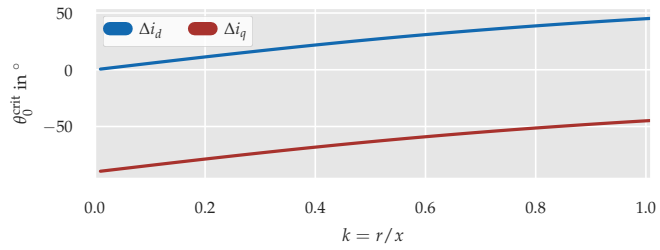

Fig. 8. Critical angle as a function of R/X ratio for control with Δi_d and Δi_q.

that the change in voltage magnitude is higher than the initial change in current.

For IBR control with i_d, Fig. 7 illustrates the consequences of operating at the critical angle. For $k = 0.013$, the critical angle is close to 0, as indicated by Fig. 8. During low loading conditions, small changes in d-axis current cause large voltage magnitude deviations and endanger IBR stability. Grid-following devices need a voltage reference signal to synchronize, but difficulties arise when large voltage oscillations occur. Consequently, devices face issues synchronizing and may disconnect during such conditions.

The position of the singularity and critical angle shifts with the R/X ratio as suggested by Fig. 7 and Fig. 8. For higher k, the critical operating condition for IBR control through i_d shifts to higher initial loading.

V. Implication for Real-World Systems

The analytical discussion suggests that the R/X, external grid strength, and voltage angle at the PCC significantly affect the IBR performance and that some loading conditions might cause small-signal instability at the IBR terminal.

Distinct differences in IBR operation in TNs and DNs occur. Higher damping is expected for IBRs in DN systems, while those in TN systems are more prone to oscillations due to lower R/X, higher resonance gain, and higher damping factor. Our analytical discussions highlight that system damping is a key contributing factor to the secure operation of IBR-rich TNs. This also means that system damping should be considered in future system planning for security purposes. In addition, our analysis implies that small-signal oscillations may not be a severe issue for IBRs connected to DNs. Furthermore, in DNs, a coupling between i_d and V, and i_q and θ is expected, which is different from operation in strong TN systems. Under these conditions, decoupling frequency and active power studies from voltage and reactive power studies is no longer valid. Since decoupling no longer holds, there may be a need for detailed dynamic modeling of IBR-rich DNs.

Independent of the voltage level, low loading conditions appear critical. The traditionally studied coupling between i_d and θ and i_q and V exhibits high sensitivity during these conditions, no matter the R/X ratio. As a result, IBRs might face problems in staying synchronized. From an industry perspective, this issue is now being discussed and referred to as minimum *operational demand security* challenges [19].

In addition, the results indicate that for a specific grid impedance and R/X ratio, critical operating conditions in terms of a critical voltage angle exist. These conditions should be tested when IBRs are integrated into ancillary service markets and are supposed to participate in frequency/voltage control. The analytic results indicate that voltages are extremely sensitive to changes in IBR current for some loading conditions. Under these conditions, the IBRs might destabilize themselves and harm other units in the area.

VI. Conclusion

This paper presents analytical discussions on IBR small-signal stability in varying grid conditions. The derived transfer functions and subsequent small-signal analysis hold for any inverter-based technology.

When IBRs are used for grid support in a grid-following control fashion, the grid characteristics at the PCC severely influence the IBR's small-signal stability and synchronism. The analytic derivation indicates that critical operating conditions exist given a particular R/X and grid strength at the PCC. The mentioned system-level aspects should be further investigated and considered when defining IBR grid-code requirements in future system operations. We have also highlighted that system damping is a key contributing factor to the secure operation of IBR-rich TNs. At the same time, it may be a manageable issue in IBR-rich DNs. It is then advisable to include system damping when planning the security of future TNs.

References

[1] M. G. Dozein, *System dynamics of low-carbon grids: Fundamentals, challenges, and mitigation solutions*. PhD thesis, The University of Melbourne, Australia, 2021.
[2] N. Hatziargyriou, J. Milanovic, C. Rahmann, V. Ajjarapu, C. Canizares, I. Erlich, D. Hill, I. Hiskens, I. Kamwa, B. Pal, P. Pourbeik, J. Sanchez-Gasca, A. Stankovic, T. Van Cutsem, V. Vittal, and C. Vournas, "Definition and classification of power system stability – revisited & extended," *IEEE Trans. Power Sys.*, vol. 36, no. 4, pp. 3271–3281, 2021.
[3] "Ieee standard for interconnection and interoperability of inverter-based resources (ibrs) interconnecting with associated transmission electric power systems," *IEEE Std 2800-2022*, 2022.
[4] National Grid ESO, "NOA Stability Pathfinder Phase 3, technical performance requirements," Nov 2020.
[5] M. Chen, D. Zhou, A. Tayyebi, E. Prieto-Araujo, F. Dörfler, and F. Blaabjerg, "Generalized multivariable grid-forming control design for power converters," *IEEE Trans. Smart Grid*, vol. 13, no. 4, pp. 2873–2885, 2022.
[6] D. B. Rathnayake and B. Bahrani, "Multivariable control design for grid-forming inverters with decoupled active and reactive power loops," *IEEE Trans. Power Electron.*, vol. 38, no. 2, pp. 1635–1649, 2023.
[7] "Ieee standard for interconnection and interoperability of distributed energy resources with associated electric power systems interfaces," *IEEE Std 1547-2018 (Revision of IEEE Std 1547-2003)*, 2018.
[8] Australian Energy Market Commission (AEMC), "Investigation into system strength frameworks in the NEM," 2020.
[9] NERC, "PSB-connected inverter-based resource performance," 2018.
[10] U. Markovic, J. Vorwerk, P. Aristidou, and G. Hug, "Stability analysis of converter control modes in low-inertia power systems," in *2018 IEEE PES ISGT-Europe*, 2018.
[11] M. Ghazavi Dozein, B. C. Pal, and P. Mancarella, "Dynamics of inverter-based resources in weak distribution grids," *IEEE Trans. Power Sys.*, vol. 37, no. 5, pp. 3682–3692, 2022.
[12] AEMO, "West Murray," 2018. www.aemo.com.au/en/energy-systems/electricity/national-electricity-market-nem/participate-in-the-market/network-connections/west-murray.
[13] L. Fan, Z. Miao, S. Shah, Y. Cheng, J. Rose, S.-H. Huang, B. Pal, X. Xie, N. Modi, S. Wang, and S. Zhu, "Real-world 20-hz ibr subsynchronous oscillations: Signatures and mechanism analysis," *IEEE Trans. Energy Convers.*, pp. 1–11, 2022.
[14] M. Paolone, T. Gaunt, X. Guillaud, M. Liserre, S. Meliopoulos, A. Monti, T. Van Cutsem, V. Vittal, and C. Vournas, "Fundamentals of power systems modelling in the presence of converter-interfaced generation," *Electric Power Systems Research*, vol. 189, 2020.
[15] AEMO, "Final report-Queensland and South Australia system separation on 25 august 2018," 2019.
[16] P. Kundur, *Power System Stability and Control*. McGraw-Hill, 1994.
[17] A. J. Schwab, *Elektroenergiesysteme*. Berlin: Springer Vieweg, 2020.
[18] G. F. Franklin, *Feedback control of dynamic systems*. Always learning, Boston: Pearson, seventh edition, global edition. ed., 2015.
[19] AEMO, "Smart Meter Backstop Mechanism Capability Trial, Phase 2 Evaluation Report," 2022.

VII. Thermal Loads: Constraints

A. Simplified

Temperature inside the chamber:

$$\dot{T}_c = \alpha(T_a - T_c(t)) - \beta P(t) + w(t) \tag{6a}$$

$$T_c(t) = T_{co} + T_a\left(1 - e^{-\alpha t}\right) + e^{-\alpha t}\int_{t_0=0}^{t} \left[-\beta P_m(\xi) + w(\xi)\right] d\xi \tag{6b}$$

where

- T_c is the chamber internal temperature
- T_a is the ambient temperature
- $P(t)$ is the power input to the compressor that equals the motor power $P_m(t)$
- $\alpha = \frac{1}{R_{\text{th}} C_{\text{th}}}$, with R_{th} and C_{th} are the thermal resistance and conductance
- $\beta = \frac{\text{COP}}{C}$, where COP is the coefficient of performance

Assume:

- constant COP, but it is a function of P or rotational motor speed ω
- lossless power conversion across the inverter stages, so that the terminal power $P_t = P_m = v_d i_q$
- the q-axis voltage at the terminal is zero, $v_q = 0$ as controlled by the PLL
- the q-axis current at the terminal is zero, $i_q = 0$, because of unity-power factor control
- no disturbances to the chamber $w(t) = 0$

Then it follows:

$$\begin{aligned} T_{\text{c,min}} - T_{co} - T_a\left(1 - e^{-\alpha t}\right) \le -\beta e^{-\alpha t}\int_{t_0=0}^{t} v_d(\xi) i_d(\xi)\, d\xi \\ \le T_{\text{c,max}} - T_{co} - T_a\left(1 - e^{-\alpha t}\right) \end{aligned} \tag{7}$$

or

$$\Delta T_c = T_a\left(1 - e^{-\alpha t}\right) - \beta e^{-\alpha t}\int_{t_0=0}^{t} v_d(\xi) i_d(\xi)\, d\xi \tag{8}$$

If we assume that a service needs to be provided for a specified duration t_s, the power that can be sustained for the entire service duration is:

$$P_s = \frac{1}{\beta t_s}\left[e^{\alpha t_s}(T_a - \Delta T_{c,max}) - T_a\right] \tag{9}$$

where we have assumed that the power is constant throughout the service period, and $\Delta T_{\text{c,max}}$ is the maximum acceptable temperature change in the controlled chamber.

Conclusions:

- power support limited by the ambient temperature, thermal properties and the maximum permissible temperature change
- sign convention selected for refrigerator or cooling device
- for cooling device:
  - power is higher for low COPs
  - power is higher for higher thermal capacity

For a standard refrigerator:

TABLE II
Some standard refrigeration parameters

Parameter	T_a	α	β
Value	$20°C$	$[4,6]\cdot 10^{-5} s^{-1}$	$4.4\cdot 10^{-5} °C/kJ$

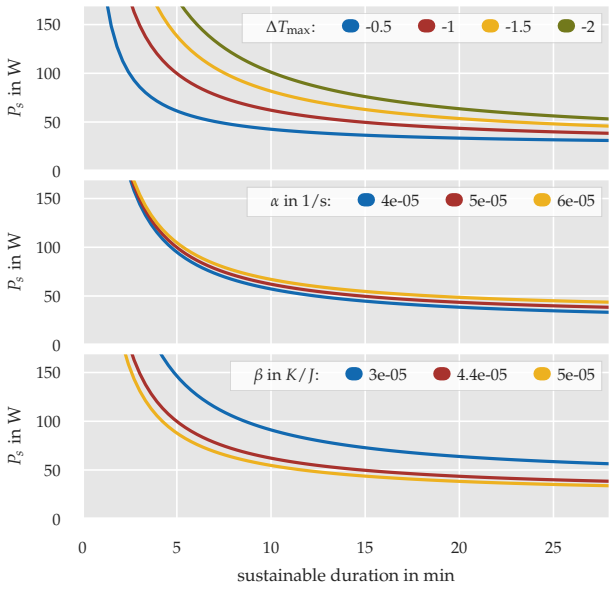

Fig. 9. Acceptable power changes P_s and their sustainable duration for different thermal parameterizations. Parameter ranges taken from Vaggelis PhD Thesis. $P_s > 0$ means increase in load power, $P_s = 0$ means no power supplied to the refrigerator.

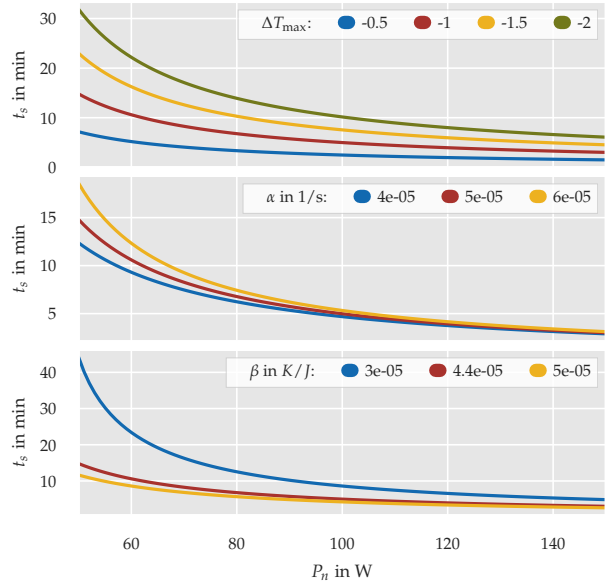

Fig. 10. Sustainable service duration t_s depending on the of nominal power P_n for different refrigeration parameterizations and acceptable temperature changes ΔT_{max}.

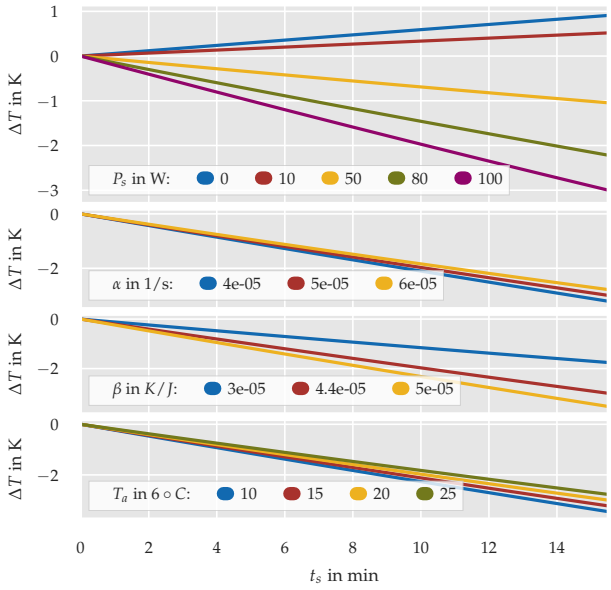

Fig. 11. Temperature deviation ΔT in a refrigerator as a function of reserve provision duration t_s for different parameterizations. $P_s = 0$ means the refrigerator is switched off, while $P_s > 0$ means the refrigerator supplies positive reserve.

VIII. Battery

Energy content must remain within:

$$E_n \text{SOC}_{\min} \leq E(t) \leq E_n \text{SOC}_{\max} \tag{10}$$

where SOC is the state of charge, $E(t)$ is the energy at time t, and E_n is the nominal capacity of the battery.

The energy over time can be computed as:

$$E(t) = E_0 + \int_{t_0=0}^{t} P(\xi)\, d\xi \tag{11}$$

If the battery does not provide any reactive power support, and is controlled to a power factor of 1, then with $P = v_d i_d$ it follows:

$$E_n \text{SOC}_{\min} \leq E_0 + \int_{t_0=0}^{t} v_d(\xi) i_d(\xi)\, d\xi \leq E_n \text{SOC}_{\max} \tag{12}$$

otherwise:

$$E_n \text{SOC}_{\min} \leq E_0 + \int_{t_0=0}^{t} \left[v_d(\xi) i_d(\xi) + v_q(\xi) i_q(\xi)\right] d\xi \leq E_n \text{SOC}_{\max} \tag{13}$$

Thus, the power that can be sustained for a required support duration t_s equals:

$$P_s = \Delta E_{\max} t_s^{-1} \tag{14}$$

and solely depends on the maximum permissible energy change.

Consider Hornsdale Power reserve: P_n =150 MW, E_n =129 MWh

If initially at 0.5 SOC and allowed to range in between 0.2 and 0.8 ($\Delta E_{\max} = 0.3 E_n$), then maximum duration is:

$$t_s = \frac{\Delta E_{\max}}{P_n} = \frac{0.3 \cdot 129 \text{ MWh}}{150 \text{ MW}} = 15.48 \text{ min} \tag{15}$$

If initially at one end of the acceptable SOC, then duration can be extended, e.g. if initially at 0.2 and allowed to go to 0.8, then t_s= 30 min. However in such a scenario only one direction of reserve possible.